Published in final edited form as:

Nat Cell Biol. 2009 April ; 11(4): 443–450. doi:10.1038/ncb1851.

Myosin IIIa boosts elongation of stereocilia by transporting espin 1 to the plus ends of actin filaments

Felipe T. Salles[1,*], **Raymond C. Merritt Jr.**[1,2,*], **Uri Manor**[1], **Gerard W. Dougherty**[1,5], **Aurea D. Sousa**[1], **Judy E. Moore**[3], **Christopher M. Yengo**[3], **Andréa C. Dosé**[4], and **Bechara Kachar**[1]

[1]Laboratory of Cell Structure and Dynamics, National Institute on Deafness and Other Communication Disorders, National Institutes of Health, Bethesda, MD 20892, USA.

[2]Department of Biology, University of Maryland, College Park, MD 20742, USA.

[3]Department of Biology, University of North Carolina at Charlotte, Charlotte, NC 28223, USA

[4]Department of Molecular and Cell Biology, University of California, Berkeley, CA 94720, USA.

Keywords

hair cells; myosin IIIa; actin protrusion; length regulation; filopodia; stereocilia; hearing; espin; deafness; WH2 motif; actin polymerization; MYO3A; ESPN

Two proteins implicated in inherited deafness, myosin IIIa1, a plus end directed motor2, and espin3–5, an actin bundling protein containing the actin-monomer-binding motif WH26, have been shown to influence the length of mechanosensory stereocilia7, 8. Here we report that espin 1, an ankyrin repeat-containing isoform of espin6, colocalizes with myosin IIIa at stereocilia tips and interacts with a unique conserved domain of myosin IIIa. We show that overexpression of these proteins causes elongation of stereocilia greater that when myosin IIIa alone or espin 1 alone are overexpressed. When these two proteins are co-expressed in the fibroblast-like COS-7 cell line they induce a ten-fold elongation of filopodia. This extraordinary filopodia elongation results from the transport of espin 1 to the plus ends of F-actin by myosin IIIa and depends on espin 1 WH2 activity. This study provides the basis for understanding the role myosin IIIa and espin 1 play in regulating stereocilia length, and presents a physiological example where myosins can boost elongation of actin protrusions by transporting actin regulatory factors to the plus ends of actin filaments.

Send Correspondence to: Bechara Kachar, M.D., Laboratory of Cell Structure and Dynamics, NIDCD, National Institutes of Health, Bldg.: 50, Room: 4249, 50 South Drive Bethesda, MD 20892-8027, Tel.: (301) 402-1600; Fax: (301) 402-1765, Email: kacharb@nidcd.nih.gov.

*Contributed equally

[5]Current address: Consorzio Mario Negri Sud, Department of Cell Biology and Oncology, Santa Maria Imbaro, Chieti, Italy 66030.

Author Contributions: R.C.M. designed probes and experiments, performed the GST pull-downs, cell culture, immunocytochemistry, and transfections; F.T.S. performed the dissections, cell and organotypic cultures, immuno-histochemistry, transfections, and confocal imaging; G.W.D. and A.C.D. designed probes, performed transfections, and contributed to experimental design; U.M. performed image and statistical analyses; A.D.S. characterized antibody and DNA probes; C.M.Y. and J.E.M. generated myosin IIIa kinase dead cDNA, purified, and performed kinase and motor activity assays.; B.K. performed electron microscopy, designed experiments, and analyzed the results together with all the other authors. All authors discussed and helped prepare the manuscript.

Stereocilia, the prominent actin protrusions on the apical surfaces sensory hair cells, emerge early during development and their lengths are maintained at fixed heights for the lifetime of the organism. The bundle of parallel actin filaments that make up the core of each stereocilium is continuously renewed, with the entire actin bundle constantly assembled at the tip, treadmilling downward, and disassembling at the base9–11. Given that stereocilia can be up to 100 μm in length, it is likely that some form of regulated transport is necessary to localize components of the actin polymerization machinery to the plus end of the actin filaments. Although several myosins have been shown to alter stereocilia lengths and shapes depending on their expression levels9, 12–16, the mechanisms by which these motors or their binding partners regulate actin dynamics and stereocilia lengths remain unclear.

Using antibodies specific to the ankyrin repeat domain (ARD) of espin 1 (Supplementary Information, Fig. S1), we show localization at stereocilia tips with a tip-to-base gradient distribution (Fig. 1) similar to what was previously described for myosin IIIa. The immunofluorescence of espin 1 is more intense in the longer stereocilia and the characteristic tip-to-base fluorescence intensity gradient has a longer decay length (Fig. 1g,h). In contrast to other espin isoforms, which are present inside the actin core and along the entire stereocilia length8, espin 1 is excluded from the actin cores and forms a thimble-like distribution at the tips of stereocilia (Fig. 1). Immunofluorescence in developing hair cells of the rat organ of Corti shows that espin 1 can be detected at the tips of stereocilia during their elongation and maturation phases (Fig. 1k–m). To confirm the localization of espin 1 at the tips of stereocilia, we overexpressed GFP-espin 1 in organotypic cultures of hair cells. Transfected hair cells show that GFP-espin 1 localizes at the tips of stereocilia, exhibiting a tip-to-base gradient of intensity (Fig. 2) comparable to the immunolocalization (Fig. 1). These localization patterns – tip-to-base gradients and thimble-like distributions7, as well as the temporal expression pattern17 – closely match those of myosin IIIa. We hypothesized that targeting espin 1 to stereocilia tips, which is the site of actin polymerization9, 11, influences actin polymerization and stereocilia elongation. An analysis of the heights of stereocilia of cochlear and vestibular hair cells transfected with GFP-espin 1 shows elongation of stereocilia upon overexpression of espin 1 (Fig. 2), consistent with our hypothesis.

The striking similarity of the tip-to-base gradient localization of both espin 1 and myosin IIIa prompted us to investigate whether myosin IIIa helps localize espin 1 to the tips of stereocilia and whether they have a combined role in the regulation of stereocilia length. We compared stereocilia length in hair cells transfected with espin alone, myosin IIIa alone and with a combination of both plasmids (Fig. 2). Hair cells transfected with myosin IIIa and espin 1 show an increase in stereocilia length, higher than the combined increase observed for myosin IIIa alone and espin 1 alone (Fig. 2). It is important to note that any analysis of lengthening due to overexpression of myosin IIIa and espin 1 in hair cells must take into account intrinsic limitations due to natural stereocilia length variations and, importantly, the fact that stereocilia are already quite elongated and express robust amounts of endogenous espin 1 and myosin IIIa.

We tested whether myosin IIIa can effectively interact with and transport espin 1 in COS-7 cells, using filopodia as a model to study actin protrusions. Myosin IIIa and espin 1 are not

naturally expressed at detectable levels in COS-7 cells 7. Myosin IIIa has been shown to induce filopodial actin protrusions and localize to their tips in cultured cells particularly well when its kinase domain has been removed (myosin IIIa ΔK)77, 18 suggesting that the kinase could serve to down-regulate the functional activity of myosin IIIa. We examined the distribution of co-expressed mCherry-ARD of espin 1 with GFP-tagged myosin IIIa ΔK (Fig. 3). We also co-expressed mCherry-ARD with GFP-tagged myosin X and GFP-tagged myosin XVa. Since all of these myosins accumulate at the tips of filopodia13, 16, 19, they provide a well-defined spatial compartment where any potential interaction can be clearly visualized. Co-transfections showed that mCherry-ARD is efficiently targeted to the tips of filopodia initiated by myosin IIIa ΔK, but not by myosins X or XVa (Fig. 3a), demonstrating a specific colocalization of ARD with myosin IIIa. Live imaging of COS-7 cells transfected with GFP-myosin IIIa ΔK and mCherry-ARD showed dynamic colocalization at the filopodia tips from the early steps of their initiation and elongation (Fig. 3b; Supplementary Information, Video S1). Live imaging also showed matching forward and rearward intra-filopodial movements of the GFP-myosin IIIa ΔK and mCherry-ARD fluorescence puncta while maintaining steady-state tip-to-base distributions (Supplementary Information, Video S2 and Video S3, and Fig. 3c), similar to the distributions of myosin IIIa and espin 1 observed in stereocilia (Fig. 1 and Fig 2). The intensity profiles for mCherry-ARD and GFP-myosin IIIa ΔK within each frame of the video (Fig. 3c) are highly correlated (cross-correlation = ∼0.990), supporting the model that these two proteins are trafficking together in the filopodia. The interaction between espin 1 ARD and myosin IIIa ΔK was confirmed with a GST pull-down assay (Fig. 3e). The dynamic localization of espin 1 ARD at filopodia tips when co-transfected with myosin IIIa, but not with myosin X or with myosin XVa, along with our GST pull-down assay results, led us to hypothesize that myosin IIIa transports espin 1 to the tips of stereocilia.

We next asked which specific region of myosin IIIa is involved in the interaction with espin 1. Myosin IIIa has two conserved tail homology domains, designated as 3THDI and 3THDII20. We first co-transfected COS-7 cells with espin 1 and GFP-myosin IIIa and showed that the two proteins colocalize at actin bundles as well as at filopodia tips (Fig. 4a,b). This pattern of colocalization is abolished when we use a GFP-myosin IIIa construct that lacks the portion of the tail containing both 3THDI and 3THDII (GFP-myoIIIa Δ32; Supplementary Information, Table S1, Fig. S2; Fig. 4a,b). We next co-transfected COS-7 cells with espin 1 and with a GFP tagged tail portion lacking 3THDII (GFP-tailΔ3THDII; Fig. 4a,b) and narrowed down the region of interaction to the 3THDI and its immediate flanking regions. We observed colocalization of espin 1 with GFP-myosin IIIa tail that contained only the 3THDI domain (GFP-3THDI; Fig. 4a,b), but not with regions of only the myosin IIIa tail immediately amino-terminal (pre3THDI) or carboxyl-terminal (post3THDI) to the 3THDI domain (Fig. 4a,b). This suggests that the 3THDI domain is necessary for the myosin IIIa:espin 1 interaction. Together these data suggest that espin 1 and myosin IIIa specifically interact via their ARD and 3THDI domains, respectively. We verified this interaction *in vitro* using a GST pull-down assay and demonstrate that GST-ARD binds to GFP-3THDI, but not to the pre3THDI or post3THDI regions (Fig. 4c).

The fact that stereocilia length can be influenced by either espin 13, 8 or myosin IIIa7, along with the observation that they both localize to the same compartment at stereocilia tips and interact biochemically, suggests a combined functional role for the myosin IIIa:espin 1 complex in the elongation of stereocilia F-actin. We discovered that COS-7 cells co-transfected with myosin IIIa ΔK and espin 1 (Fig. 5a–c) display filopodial actin protrusions that can be up to ten times longer (mean length = 14.3 ± 9.1 μm; number of cells, n_c =18; number of filopodia, n_f=56) than those transfected with myosin IIIa ΔK alone (1.7 ± 0.83 μm, n_c=12, n_f=49), or with espin 1 alone (1.3 ± 0.28 μm, n_c=13, n_f=104). Mean lengths of filopodia of COS-7 cells transfected with empty GFP vector was 1.26 ± 0.7 (n_c = 10, n_f = 59). The synergistic effect between myosin IIIa and espin 1 is specific for myosin IIIa, since we found no enhanced elongation when espin 1 was co-expressed with either myosin X (2.40 ± 1.50 μm, n_c=16, n_f=165) or myosin XVa (2.08 ± 1.63 μm, n_c=15, n_f=134).

We used myosin IIIa without the kinase domain to observe the behavior of the dephosphorylated and more functionally active myosin. To exclude the possibility that the deletion of the kinase domain produces aberrant behavior, we developed a kinase-dead construct, myosin IIIa K50R (Supplementary Information, Table. S1). This construct allowed us to examine the role of autophosphorylation in the regulation of motor function, which in turn enabled us to investigate the role of myosin IIIa motor function in espin 1 tip-localization activity. We have determined that inactivation of the myosin IIIa kinase in a myosin IIIa 2IQ construct reduces the K_{ATPase} yet it does not affect maximal ATPase activity (Supplementary Information, Table S2 and Figure S3). We next evaluated the role of the kinase activity in myosin IIIa tip-localization in COS-7 cells using GFP tagged constructs. Full-length myosin IIIa K50R localizes more efficiently to the tips of filopodia in COS-7 cells (39% at tips n_c=137) than wild-type (5% at tips n_c=200), although not as strikingly as myosin IIIa ΔK (93% at tips n=105). Furthermore, co-expression of myosin IIIa K50R and espin 1 (Fig. 5e) yielded longer filopodia (mean length = 5.93 ± 3.10 μm, n_c=15, n_f=89) than co-expression of wild-type myosin IIIa and espin 1 (3.7 ± 3.2 μm, n_c=15, n_f=63; Fig. 5d), although not as long as the myosin IIIa ΔK:espin 1 co-expression. This data shows that myosin IIIa motor ATPase activity parallels the ability of myosin IIIa to localize to filopodia tips and to elongate filopodia when co-expressed with espin 1.

Interestingly, espin 1 co-expressed with a myosin IIIa ΔK lacking the tail domain downstream of exon 32 (myosin IIIa ΔK,33,34; Supplementary Information, Table S1, Fig. S2) resulted in slightly shorter filopodia (10.0 ± 4.74 μm, n=64; Fig. 5f) than co-expression with myosin IIIa ΔK. Using COS-7 cell co-expression and GST pull-down assays, we confirmed that the upstream portion of 3THDI (3THDI Δ33, Supplementary Information, Fig. S4) binds to espin 1. The 3THDII of myosin IIIa has previously been shown to be an actin-binding site18. Previous studies reported that myosin IIIa lacking the 3THDII actin-binding domain does not localize to filopodia tips 7, 18, but here we show that when co-expressed with espin 1 myosin IIIa goes to the tip and promotes filopodia elongation (Fig. 5f). It appears that the association with espin 1, which does have actin-binding sites, compensates for the missing actin-binding site in the myosin IIIa without the 3THDII domain.

Co-expression of espin 1 and myosin IIIa results in enhanced localization of espin 1 at filopodia tips (Supplementary Information, Fig. S5). When myosin IIIa ΔK is co-expressed with espin 1 lacking the ARD domain, we observed that both espin tip localization and filopodia elongation are abolished (Fig. 5g). These results demonstrate that the actin cross-linking activity of espin 1 is not solely responsible for the enhanced filopodia or stereocilia elongation observed in our experiments. We conclude that espin 1 promotes enhanced elongation of filopodia only when transported to the polymerization end of actin filaments by myosin IIIa. The fact that espin 1 elongates filopodia only when localized to the F-actin plus ends by myosin IIIa suggests that WH2-dependent polymerization activity is involved in elongation. We tested this hypothesis by substituting the first two of three highly conserved leucine residues of the espin 1 WH2 motif (L655A, L656A), which have been shown to be essential for its actin-monomer-binding activity21, 22. In COS-7 cells co-transfected with the WH2-mutated espin 1 construct (espin 1 mWH2) and myosin IIIa ΔK (Fig. 5h), the average length of filopodia (2.65 ±1.50 μm, n_c=10, n_f=75) remains comparable to the protrusions induced by myosin IIIa ΔK alone. The lack of enhanced elongation despite the colocalization of espin 1 mWH2 and myosin IIIa ΔK at the tips of filopodia (Fig. 5h) demonstrates that the WH2 motif is critical for mediating the role of espin 1 in elongation.

The steady-state distribution of myosin IIIa in a tip-to-base gradient is likely dynamically maintained. The length of the myosin IIIa distribution should be inversely proportional to the net velocity of the myosin towards the tip23, which will be slower for faster treadmilling actin cores (i.e. in longer stereocilia9 and filopodia24). This prediction is also consistent with our observation that wild-type myosin IIIa, which has relatively low activity, has decreased tip localization in the filopodia compared to the more active kinase mutant forms of myosin IIIa used in our experiments (Fig. 5). However, in stereocilia where the actin treadmilling is much slower, the wild-type myosin IIIa self-localizes effectively to the tip7 (Fig. 2). Similarly, the observed steady-state tip-to-base gradient distribution of espin 1 is not compatible with a model where espin 1 passively diffuses and binds to myosin IIIa resident at the tip, since this scenario would result in a homogenous distribution along the entire length of the stereocilia with no detectable concentration gradient at steady-state. The gradient distribution of espin 1 at steady-state is reminiscent of a myosin VI-driven gradient for the stereocilia membrane protein PTPRQ, and is best explained by a model that includes binding, directed transport, and diffusion of myosins and their cargo25. A more detailed consideration of this dynamic process that also accounts for actin treadmilling and plus-end directed motors predicts a similar distribution, which can be several microns long for longer stereocilia23. Thus, we favor a model where myosin IIIa:espin 1 complexes are dynamically associated with the treadmilling actin core. This model suggests that espin 1 is transported to the tips of stereocilia by myosin IIIa, whereupon it remains bound to the surface of the actin core for a period of time. Interestingly, abolishing or reducing myosin IIIa kinase activity enhances the affinity of the myosin IIIa for actin, providing further evidence that the kinase domain plays a role in regulating the myosin IIIa motor kinetics and actin-binding properties26, 27. While the myosin IIIa:espin 1 complex is tightly bound to actin, it travels back towards the base of the stereocilia along with the treadmilling actin core. In support of this model, live video imaging in transfected COS-7 cells shows fluorescent puncta of GFP-myosin IIIa ΔK and mCherry-ARD (Supplementary Information, Video S4) that move

rearwards at rates matching the rates reported for actin treadmilling in filopodia (~0.5 μm/min)24. We suggest that these puncta are stably bound to the surface of the treadmilling actin filament bundle.

It is noteworthy that the stereocilia tips are also the site of mechanoelectrical transduction (MET)28, that the myosin IIIa developmental expression level is correlated with maturation of MET in stereocilia17, and that myosin IIIa has been shown to transport components of the photoreceptor transduction machinery in *Drosophila*29, 30. We cannot exclude the possibility that the localization and dynamics of the myosin IIIa:espin 1 complex are also affected by interactions with other proteins at the stereocilia tip. Furthermore, ankyrin repeats have been shown to be promiscuous binders of membrane proteins31. It is possible that the turnover and dynamic localization of the espin 1:myosin IIIa complex are influenced by interactions with components of the MET machinery, and vice-versa.

Methods

Antibodies

Affinity-purified polyclonal antibodies (PB538 and PB539) were developed in rabbits immunized with a synthetic peptide (Princeton Biomolecules, Langhorne, PA) corresponding to the amino acid sequence (LDALPVHHAARSGKLHCLR) of the first ankyrin repeat of mouse espin 1. A similarly raised antibody specific for a region conserved in all isoforms of espin (pan-espin, PB127)8 and anti-myosin IIIa (PB638)7 antibodies have been previously described.

Immuofluorescence and microscopy

Following CO_2 anesthesia, rats, mice, and guinea pigs were euthanized in accordance to National Institutes of Health (NIH) guidelines, and their temporal bones fixed by immersion in 4% paraformaldehyde in phosphate buffered saline (PBS; pH 7.4) for 2 h at room temperature. Sensory tissue was dissected in PBS, permeabilized with 0.5% Triton X-100 for 30 min and blocked overnight at 4°C with 4% bovine serum albumin in PBS. Tissue was then incubated with primary antibody for 2 h, rinsed with PBS, stained with Alexa Fluor 488-conjugated secondary antibody (Molecular Probes, Eugene, OR) for 1 h, counterstained with 0.001 U/μl Alexa Fluor 568 phalloidin (Molecular Probes), and mounted using Prolong Antifade (Molecular Probes). Fluorescence confocal images were obtained with a Nikon microscope equipped with a 100× 1.45 numerical aperture (NA) objective and a spinning disk confocal unit (PerkinElmer, Wellesley, MA).

Electron microscopy

Rat organ of Corti or vestibular tissue were either rapidly frozen by contact with a liquid nitrogen cooled metal block in a LifeCell (The Woodlands, TX) freezing apparatus or fixed, glycerinated, and plunge frozen in Freon 22 cooled in liquid nitrogen prior to freeze-substitution in 1.5% uranyl acetate in absolute methanol at −90°C. Freeze-substituted tissues were infiltrated with Lowicryl HM-20 resin (Electron Microscopy Sciences, Hatfield, PA) at −45°C and polymerized with UV light, thin-sectioned, and immunogold labeled. Samples were viewed and photographed with a Zeiss 922 electron microscope (Peabody, MA). We

also used as control for the immunogold labeling the antibody PB288 that is unrelated to espin or to myosin IIIa (Supplementary Figure 1d).

Expression plasmids

Espin 1 (NCBI accession number NM_031475) in pSPORT1 vector was obtained from imaGenes (Berlin, Germany) and PCR cloned into pEGFP-C2 (Clontech, Mountain View, CA) and pcDNA3.1(−) (Invitrogen, Carlsbad, CA) via *Eco*RI and *Kpn*I sites. The site-directed leucine-to-alanine mutations in the WH2 motif of espin 1 were generated using a GeneTailor Site-Directed Mutagenesis kit (Invitrogen). The ankyrin repeats domain between amino acid positions 16 and 363 was PCR amplified using the mouse espin 1 template (NM_207687) and subcloned in-frame into the mCherry-C1 (Clontech) expression vector via *Xho*I and *Eco*RI sites, and pDEST™ 15 GST expression vector (Invitrogen) via the Gateway LR Clonase cloning method (Invitrogen). The GFP-tagged expression plasmids used were espin 1 ΔARD (a gift from Dr. James Bartles, Northwestern University, Chicago IL), myosin X (a gift of Dr. Richard Cheney, UNC, Chapel Hill NC), myosin XVa (a gift of Dr. Thomas Friedman, NIDCD/NIH), as well as full-length and deletion constructs of myosin IIIa that were generated in our laboratories. Myosin IIIa 2IQ ΔK constructs were generated as previously described (26, 34). Myosin IIIa 2IQ K50R and myosin IIIa K50R constructs were generated by performing site-directed mutagenesis on the myosin IIIa 2IQ and myosin IIIa full length constructs, respectively. All expression plasmids were sequence verified. Further details about the clones used are located in Supplementary Information, Table S1 and Figure 3.

Cultures and transfection of COS-7 cells

COS-7 (ATCC, Manassas, VA) cells were plated on coverslips and maintained at 37°C in DMEM with 10% FBS. Cultures were transfected using GeneJuice Transfect Reagent (Novagen, San Diego, CA), incubated for 24 h. Time lapse videos of live cells were acquired at maximum nominal laser power and camera gain allowed by the confocal microscope. Samples were also fixed for 20 min in 4% paraformaldehyde in PBS, permeabilized for 30 min in 0.5% Triton X-100 in PBS, and counterstained or processed for immunofluorescence as described above.

Cultures and transfection of rat inner ear tissue

Organ of Corti and vestibular tissue were dissected from postnatal day 0–4 rats and attached to coverslips previously coated with 150 μg/μl of Cell-Tak (BD Biosciences, San Jose, CA). Cultures were maintained in DMEM/F12 (Invitrogen) with 5–7% Fetal Bovine Serum (FBS) and 1.5 μg/ml ampicillin (Sigma, St. Louis, MO) and kept at 37°C and 5% CO_2. For transfections, 50 μg of DNA was precipitated onto 25 mg of 1 μm gold particles and loaded into the Helios Gene Gun cartridges (BioRad, Hercules, CA). Tissue explants were transfected with the gene gun set at 95 psi of helium and maintained in culture for 18–48 hours. Samples were fixed and counterstained for confocal microscope viewing as described above. The efficiency of transfection ranged from 0 to 9 hair cells per explant.

Image Analysis

Image analyses was performed with ImageJ software (NIH). To estimate the relative increase in stereocilia length we compared the heights of the tallest row of well-preserved stereocilia of cochlear and vestibular hair cells transfected (H_t) with the averaged height of all their respective neighboring (usually between 3 to 5) non-transfected cells (H_{nt}) within the field of view of our camera/confocal setup (30×45 μm). The average ratio of stereocilia length was calculated as $\ell = \frac{H_T}{H_{NT}}$. ANOVA analysis was performed using MATLAB (Mathworks, Nantick, MA). Cross-correlation analysis for the intensity plot in figure 3 was performed using Microsoft Excel.

Western blots

100 mm dishes of transfected semi-confluent COS-7 cells were rinsed in PBS and scraped in 160 μl of lysis buffer: PBS, 1% Triton-X, 5 mM DTT, 1 mM Pefabloc, 5 μg/ml pepstatin A, 5 μg/ml leupeptin, 2 mM EDTA, 0.2 mM PMSF and 1% mammalian protease inhibitor cocktail (Sigma). After addition of 1x loading sample buffer and DTT (Invitrogen), samples were boiled and 10 μl of lysates were loaded in 4–12% Bis-Tris minigel (Invitrogen). Western blots were incubated overnight at 4°C with 4 μg/ml of the primary antibody. Horseradish peroxidase-conjugated goat anti-rabbit antibodies (Santa Cruz) and ECL chemiluminescence system (Amersham) were used for detection.

GST pull-down assays

Protein expressions of glutathione S-transferase (GST) alone or fused to ankyrin repeats domain (GST-ARD) were optimized under L-arabinose induction in BL21-AI bacteria (Invitrogen). GST proteins were purified from bacterial extracts using glutathione–Sepharose 4B beads according to manufacturer's instructions (Amersham Biosciences, Buckinghamshire, UK). GFP-myosin IIIa ΔK, - pre3THDI, -3THDI, and -post3THDI proteins were extracted from 24 h COS-7 transfectants via brief sonication and 20-min ultracentrifugation at 145,000 g in ice-cold lysis buffer (1% Triton X-100, 5 mM DTT, 150 mM NaCl, 50 mM Tris pH 7.4, 2 mM EDTA, 3 mM Pefabloc SC, 1x Pefabloc (Roche, Indianapolis, IN), and 1x Mammalian Protease Inhibitor cocktail (Sigma). To test for myosin IIIa interactions, the same amount of GST-ARD or GST alone was bound to 4B beads for 1 h at 4°C followed by incubation with the GFP-tagged myosin IIIa fragment in CLB for 2 h. The beads were then washed four times with lysis buffer, and bound proteins separated by electrophoresis on NuPAGE Bis-Tris 4–12% gels (Invitrogen), and analyzed by Western blotting using rabbit polyclonal anti-GFP and anti-GST antibodies (Invitrogen).

ATPase assays

The steady-state actin-activated ATPase activity of baculovirus expressed myosin IIIa 2IQ K50R and WT were performed with the NADH coupled assay26, 32. ATPase activity of fully phosphorylated myosin IIIa was compared to unphosphorylated myosin IIIa after a 60 minute incubation at room temperature in the presence and absence of 200 μM ATP, respectively. The kinase activity of the myosin IIIa 2IQ constructs were assayed using [^{32}P]ATP or western blotting with antiphosphothreonine antibodies26, 32.

Supplementary Material

Refer to Web version on PubMed Central for supplementary material.

Acknowledgments

We thank Chi W. Pak for discussions and for the suggestion of mutations in the WH2 motif, Mark Schneider and Saeeda Latham for initial help with experiments and for discussions related to this work, Martin Horak for advice on cloning procedures, and Dr. Ronald Petralia for comments on the manuscript. This work was supported by NIDCD, DIR, NIH and in part by NIH grants # EY003575 to ACD and EY016419 to CMY.

References

1. Walsh T, et al. From flies' eyes to our ears: mutations in a human class III myosin cause progressive nonsyndromic hearing loss DFNB30. Proc Natl Acad Sci U S A. 2002; 99:7518–7523. [PubMed: 12032315]
2. Komaba S, Inoue A, Maruta S, Hosoya H, Ikebe M. Determination of human myosin III as a motor protein having a protein kinase activity. J Biol Chem. 2003; 278:21352–21360. [PubMed: 12672820]
3. Zheng L, et al. The deaf jerker mouse has a mutation in the gene encoding the espin actin-bundling proteins of hair cell stereocilia and lacks espins. Cell. 2000; 102:377–385. [PubMed: 10975527]
4. Donaudy F, et al. Espin gene (ESPN) mutations associated with autosomal dominant hearing loss cause defects in microvillar elongation or organisation. J Med Genet. 2006; 43:157–161. [PubMed: 15930085]
5. Naz S, et al. Mutations of ESPN cause autosomal recessive deafness and vestibular dysfunction. J Med Genet. 2004; 41:591–595. [PubMed: 15286153]
6. Sekerkova G, Zheng L, Loomis PA, Mugnaini E, Bartles JR. Espins and the actin cytoskeleton of hair cell stereocilia and sensory cell microvilli. Cell Mol Life Sci. 2006; 63:2329–2341. [PubMed: 16909209]
7. Schneider ME, et al. A new compartment at stereocilia tips defined by spatial and temporal patterns of myosin IIIa expression. J Neurosci. 2006; 26:10243–10252. [PubMed: 17021180]
8. Rzadzinska A, Schneider M, Noben-Trauth K, Bartles JR, Kachar B. Balanced levels of Espin are critical for stereociliary growth and length maintenance. Cell Motil Cytoskeleton. 2005; 62:157–165. [PubMed: 16206170]
9. Rzadzinska AK, Schneider ME, Davies C, Riordan GP, Kachar B. An actin molecular treadmill and myosins maintain stereocilia functional architecture and self-renewal. J Cell Biol. 2004; 164:887–897. [PubMed: 15024034]
10. Lin HW, Schneider ME, Kachar B. When size matters: the dynamic regulation of stereocilia lengths. Curr Opin Cell Biol. 2005; 17:55–61. [PubMed: 15661519]
11. Schneider ME, Belyantseva IA, Azevedo RB, Kachar B. Rapid renewal of auditory hair bundles. Nature. 2002; 418:837–838. [PubMed: 12192399]
12. Manor U, Kachar B. Dynamic length regulation of sensory stereocilia. Semin Cell Dev Biol. 2008; 19:502–510. [PubMed: 18692583]
13. Belyantseva IA, et al. Myosin-XVa is required for tip localization of whirlin and differential elongation of hair-cell stereocilia. Nat Cell Biol. 2005; 7:148–156. [PubMed: 15654330]
14. Prosser HM, Rzadzinska AK, Steel KP, Bradley A. Mosaic complementation demonstrates a regulatory role for myosin VIIa in actin dynamics of stereocilia. Mol Cell Biol. 2008; 28:1702–1712. [PubMed: 18160714]
15. Tokuo H, Mabuchi K, Ikebe M. The motor activity of myosin-X promotes actin fiber convergence at the cell periphery to initiate filopodia formation. J Cell Biol. 2007; 179:229–238. [PubMed: 17954606]
16. Tokuo H, Ikebe M. Myosin X transports Mena/VASP to the tip of filopodia. Biochem Biophys Res Commun. 2004; 319:214–220. [PubMed: 15158464]

17. Waguespack J, Salles FT, Kachar B, Ricci AJ. Stepwise morphological and functional maturation of mechanotransduction in rat outer hair cells. J Neurosci. 2007; 27:13890–13902. [PubMed: 18077701]
18. Les Erickson F, Corsa AC, Dose AC, Burnside B. Localization of a class III myosin to filopodia tips in transfected HeLa cells requires an actin-binding site in its tail domain. Mol Biol Cell. 2003; 14:4173–4180. [PubMed: 14517327]
19. Bohil AB, Robertson BW, Cheney RE. Myosin-X is a molecular motor that functions in filopodia formation. Proc Natl Acad Sci U S A. 2006; 103:12411–12416. [PubMed: 16894163]
20. Dose AC, et al. Myo3A, one of two class III myosin genes expressed in vertebrate retina, is localized to the calycal processes of rod and cone photoreceptors and is expressed in the sacculus. Mol Biol Cell. 2003; 14:1058–1073. [PubMed: 12631723]
21. Quinlan ME, Heuser JE, Kerkhoff E, Mullins RD. Drosophila Spire is an actin nucleation factor. Nature. 2005; 433:382–388. [PubMed: 15674283]
22. Loomis PA, et al. Targeted wild-type and jerker espins reveal a novel, WH2-domain-dependent way to make actin bundles in cells. Journal of cell science. 2006; 119:1655–1665. [PubMed: 16569662]
23. Naoz M, Manor U, Sakaguchi H, Kachar B, Gov N. Protein localization by actin treadmilling and molecular motors regulates stereocilia shape and treadmilling rate. Biophysical Journal. 2008 In press.
24. Mallavarapu A, Mitchison T. Regulated actin cytoskeleton assembly at filopodium tips controls their extension and retraction. The Journal of cell biology. 1999; 146:1097–1106. [PubMed: 10477762]
25. Sakaguchi H, et al. Dynamic compartmentalization of protein tyrosine phosphatase receptor Q at the proximal end of stereocilia: Implication of myosin VI-based transport. Cell Motil Cytoskeleton. 2008
26. Dose AC, et al. The kinase domain alters the kinetic properties of the myosin IIIA motor. Biochemistry. 2008; 47:2485–2496. [PubMed: 18229949]
27. Kambara T, Komaba S, Ikebe M. Human myosin III is a motor having an extremely high affinity for actin. J Biol Chem. 2006; 281:37291–37301. [PubMed: 17012748]
28. Ricci AJ, Kachar B, Gale J, Van Netten SM. Mechano-electrical transduction: new insights into old ideas. J Membr Biol. 2006; 209:71–88. [PubMed: 16773495]
29. Porter JA, Yu M, Doberstein SK, Pollard TD, Montell C. Dependence of calmodulin localization in the retina on the NINAC unconventional myosin. Science. 1993; 262:1038–1042. [PubMed: 8235618]
30. Wes PD, et al. Termination of phototransduction requires binding of the NINAC myosin III and the PDZ protein INAD. Nat Neurosci. 1999; 2:447–453. [PubMed: 10321249]
31. Mosavi LK, Cammett TJ, Desrosiers DC, Peng ZY. The ankyrin repeat as molecular architecture for protein recognition. Protein Sci. 2004; 13:1435–1448. [PubMed: 15152081]
32. Dose AC, Ananthanarayanan S, Moore JE, Burnside B, Yengo CM. Kinetic mechanism of human myosin IIIA. J Biol Chem. 2007; 282:216–231. [PubMed: 17074769]

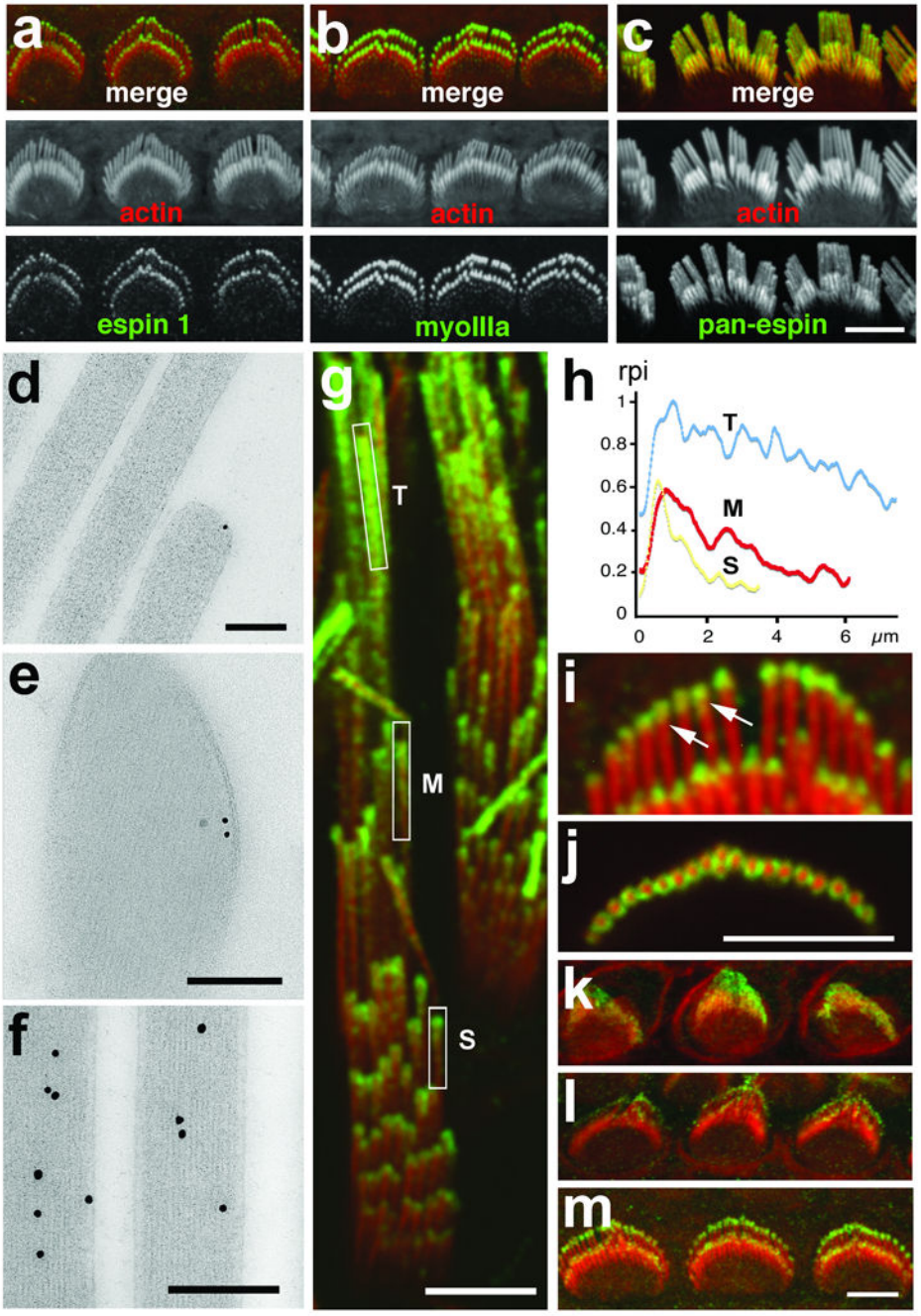

Figure 1.

Espin 1 immunofluorescence distribution in stereocilia is similar to myosin IIIa Immunofluorescence confocal images show myosin IIIa (green) localized at the tips of stereocilia in rat cochlear hair cells at PD6 (**a**) matching the localization observed for espin 1 (green, **b**). In contrast, pan-espin labeling (green) appears along the entire stereocilia (**c**). Scale bar, 5 μm. Immunogold labeling shows espin 1 localized at the tip of stereocilia around the actin core (**d, e**) in contrast to labeling with a pan-espin antibody which shows localization throughout the entire stereocilia actin cores (**f**)in directly frozen (**d**) or plunge-

frozen (**e**) adult rat cochlear (**d**) and vestibular (**e, f**) hair cells. Scale bars, 200 nm. (**g**) Immunofluorescence of espin 1 (green) localization in guinea pig vestibular stereocilia reveals a tip-to-base gradient that is more extended in longer stereocilia (inset T) than medium (inset M) and short (inset S) stereocilia. (**h**) Measurements of the green (espin 1) and red (actin) relative pixel intensity (rpi) of fluorescence along the stereocilia for each rectangular inset in **g** confirm this tip-to-base concentration gradient of espin 1 immunofluorescence. Longitudinal (**i**) as well as cross section (**j**) images reveal a thimble-like distribution of espin 1 (green) at tips of stereocilia in hair cells of P8 rat cochlea. (**k-m**) Immunofluorescence of rat cochlear hair cells in different developmental time points shows that espin 1 targets stereocilia tips as early as P0 (**k**) and undergoes progressive compartmentalization at the tips during P2 (**l**) and P4 (**m**), reaching a peak of intensity at ∼PD6 as shown in **b**. Scale bars, 5 μm. Antibodies: Espin 1 (PB539), myosin IIIa (PB638), and pan-espin (PB127). In all immunofluorescence images, the immunolabeling is visualized using Alexa-488-conjugated secondary antibody and F-actin (red) is visualized using Alexa 568-phalloidin.

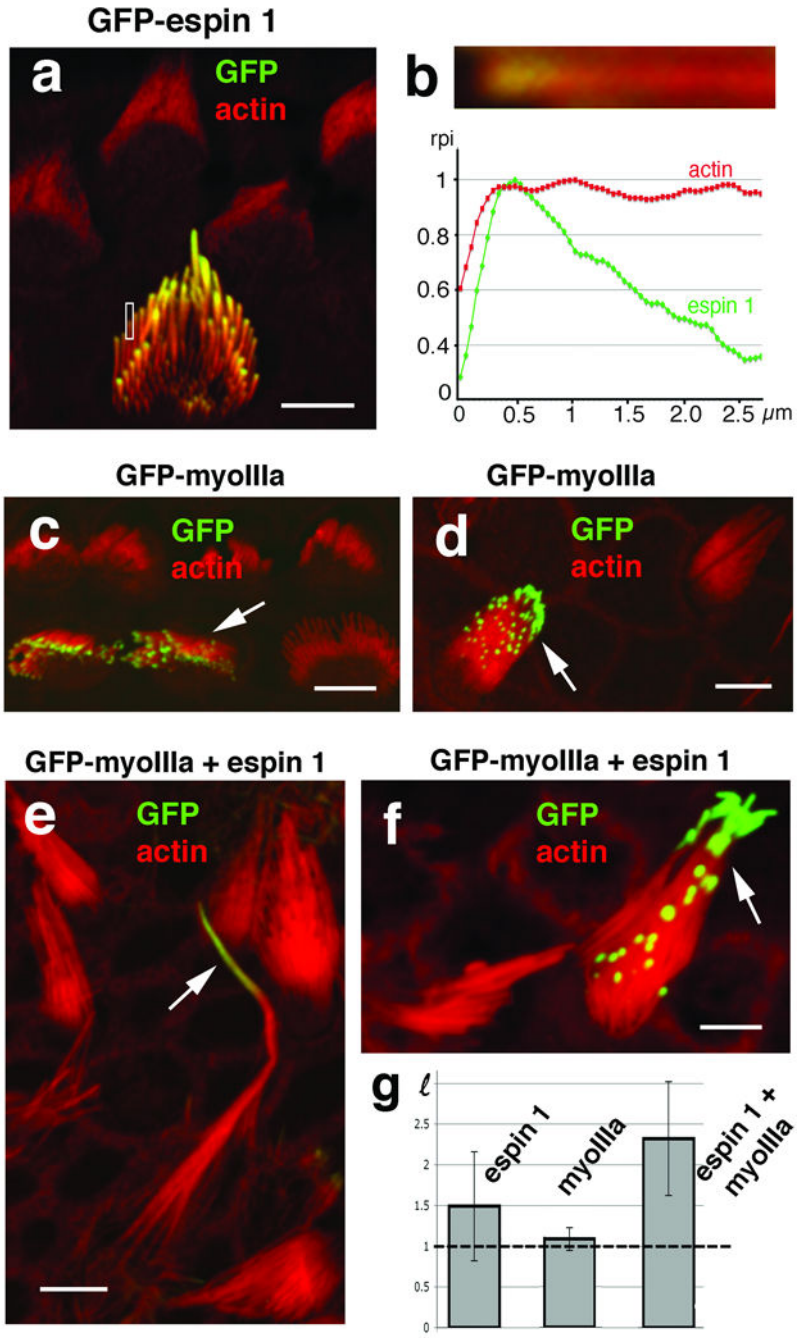

Figure 2.

Espin 1 alone or when co-overexpressed with myosin IIIa elongates stereocilia. **(a)** GFP-espin 1 localizes to stereocilia tips in a tip-to-base gradient distribution in transfected cultured organ of Corti hair cells. (**b**) High magnification close-up view and measurement of the relative pixel intensity (rpi) of GFP-espin 1 (green) and actin (Alexa 568-phalloidin, red) fluorescence along the distal portion of the stereocilia shown in the rectangular inset in (**a**) matches the tip-to-base concentration gradient observed for endogenous espin 1 (Fig. 1**h**). Organ of Corti (**c**) and vestibular (**d**) hair cells transfected with GFP-myosin IIIa show tip

localization similar to espin 1. Co-transfection of vestibular hair cells with GFP-myoIIIa (arrow, green) and untagged espin 1 together (**e** and **f**) produce longer stereocilia than hair cells transfected with GFP-espin 1 alone (**a**) or with GFP-myosin IIIa alone (**c** and **d**). The average ratios of stereocilia length between transfected (H_T) and neighboring non-transfected (H_{NT}) cells, $\ell = \frac{H_T}{H_{NT}}$, are plotted in the bar graph in (**g**). GFP-espin 1 alone = 1.5 ± 0.67, n=19 (∼50% increase); GFP-myoIIIa alone = 1.1 ± 0.14, n=16 (∼10% increase); and GFP-myosin IIIa and espin 1 = 2.3 ± 0.69, n=14, (∼130% increase). Note that a value of ℓ=1 (indicated by the dotted line in the graph) corresponds to a zero percent increase in length. The error bars represent the standard deviation of the mean. ANOVA statistical analysis shows that the mean value for the hair cells co-transfected with espin1 and myosin IIIa is significantly higher than the cells transfected with espin 1 alone, with a p-value equal to 0.002. In contrast, the mean bundle heights for hair cells transfected with myosin IIIa alone were not significantly higher than the controls, with a p-value of .149. Scale bars, 5 μm.

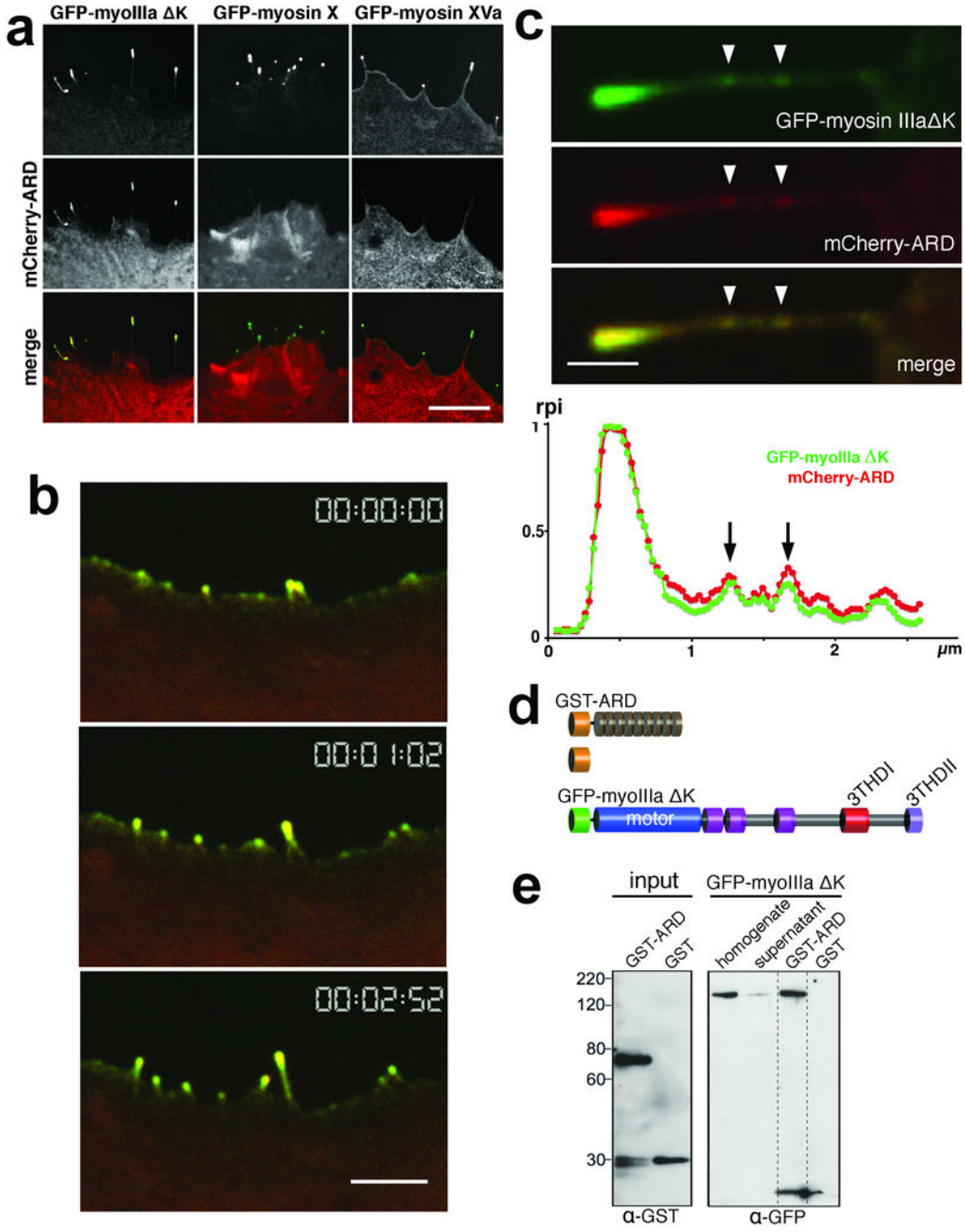

Figure 3.

Espin 1 interacts with myosin IIIa through its ankyrin repeats domain (ARD) in transfected COS-7 cells. (**a**) mCherry-tagged espin 1 ARD shows filopodia tip localization when cotransfected with GFP-myoIIIa ΔK but fails to localize at the filopodia tips when co-transfected with GFP-myosin X or GFP-myosin XVa. Scale bar, 5 μm. (**b**) Selected video images from a time lapse video (Supplementary Information, Video S1) show co-transport of GFP-myoIIIa ΔK and mCherry-ARD during the formation and extension of filopodia in COS-7 cells. Scale bar, 2.5 μm. (**c**) Single representative frame from a time lapse video of a

single filopodium (Supplementary Information, Video S2) graph with the normalized relative pixel intensity of the fluorescence along the filopodium show co-distribution (cross-correlation of the green and red intensity values = 0.990 for this frame; the average cross correlation for six randomly selected frames from the same video was 0.99) of GFP-myoIIIa ΔK and mCherry-ARD forming a tip to base gradient and co-localization of the green and red fluorescence puncta (arrowheads) corresponding to the co-transport of GFP-myoIIIa ΔK and mCherry-ARD trafficking into and out of the tip of the filopodia. Scale bar, 0.5 μm. **(d)** Schematic representation of the constructs analyzed in this figure. Legend: GST, glutathione S-transferase; GFP, green fluorescence protein; ARD, ankyrin repeats domain; myoIIIa ΔK, myosin IIIa with a deletion of it kinase domain; 3THDI and 3THDII, myosin IIIa tail homology domains 1 and 2, respectively. (**e**) Western blots of GST pull-downs show that purified GST-ARD co-precipitates with GFP-myoIIIa ΔK, but not with GST alone. Precipitates were detected using anti-GST (α-GST) and anti-GFP (α-GFP).

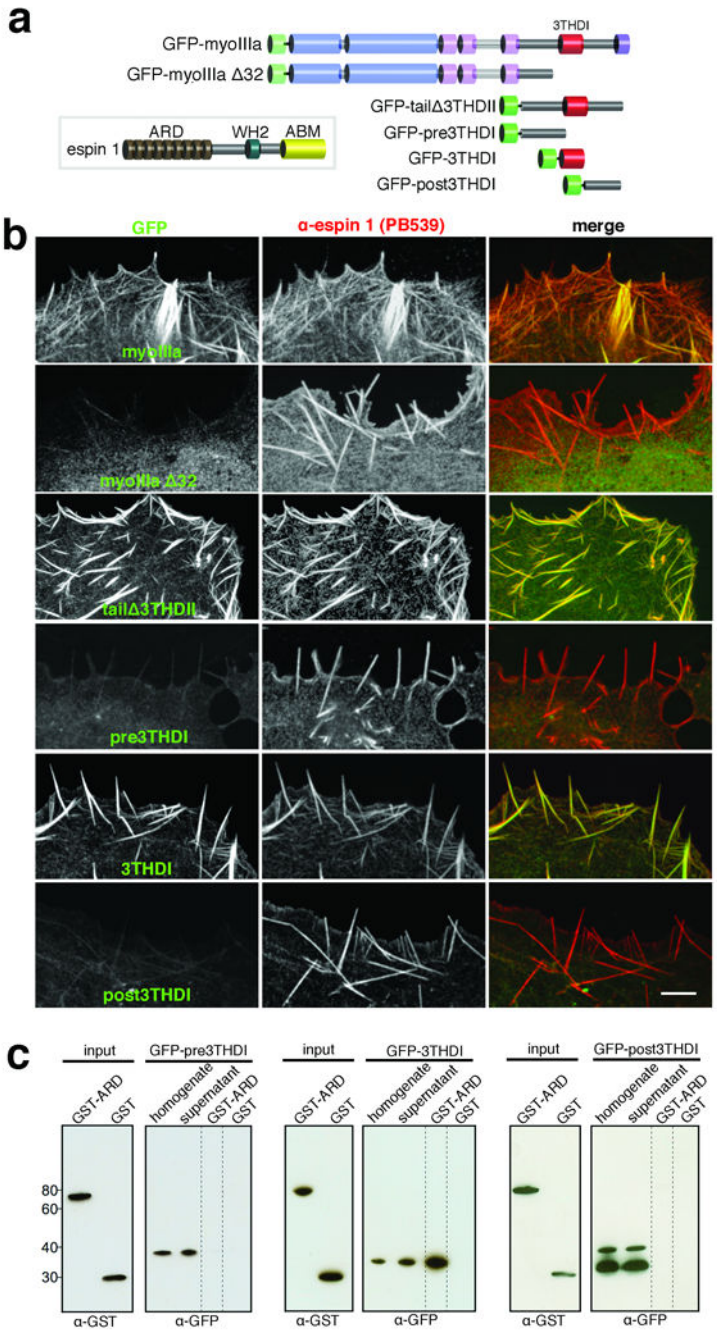

Figure 4.

Myosin IIIa interacts with espin 1 through its 3THDI domain. (**a**) Schematic representation of the espin 1 and myosin IIIa constructs analyzed in this figure. Legend: ABM, actin binding module; WH2, Wiskott-Aldrich homology domain 2; GFP-myoIIIa Δ32, myosin IIIa lacking exon 32 which causes a frame shift rendering the protein without the 3THDI and 3THDII domains. (**b**) Co-expression of untagged espin 1 shows that GFP-myoIIIa, GFP-tailΔ3THDII, and GFP-3THDI (green) colocalize with espin 1 (red) along actin filament bundles. In contrast, GFP-myoIIIa Δ32, GFP-pre-, and post3THDI are dispersed in the

cytoplasm, despite the presence of espin 1 bundles. Scale bar, 5 μm. (**c**) Western blots of GST pull-downs confirm that the 3THDI region of myosin IIIa is necessary and sufficient for binding to espin 1 ARD, as pre3THDI and post3THDI show no binding to GST-ARD. Precipitates were detected using α-GST and α-GFP.

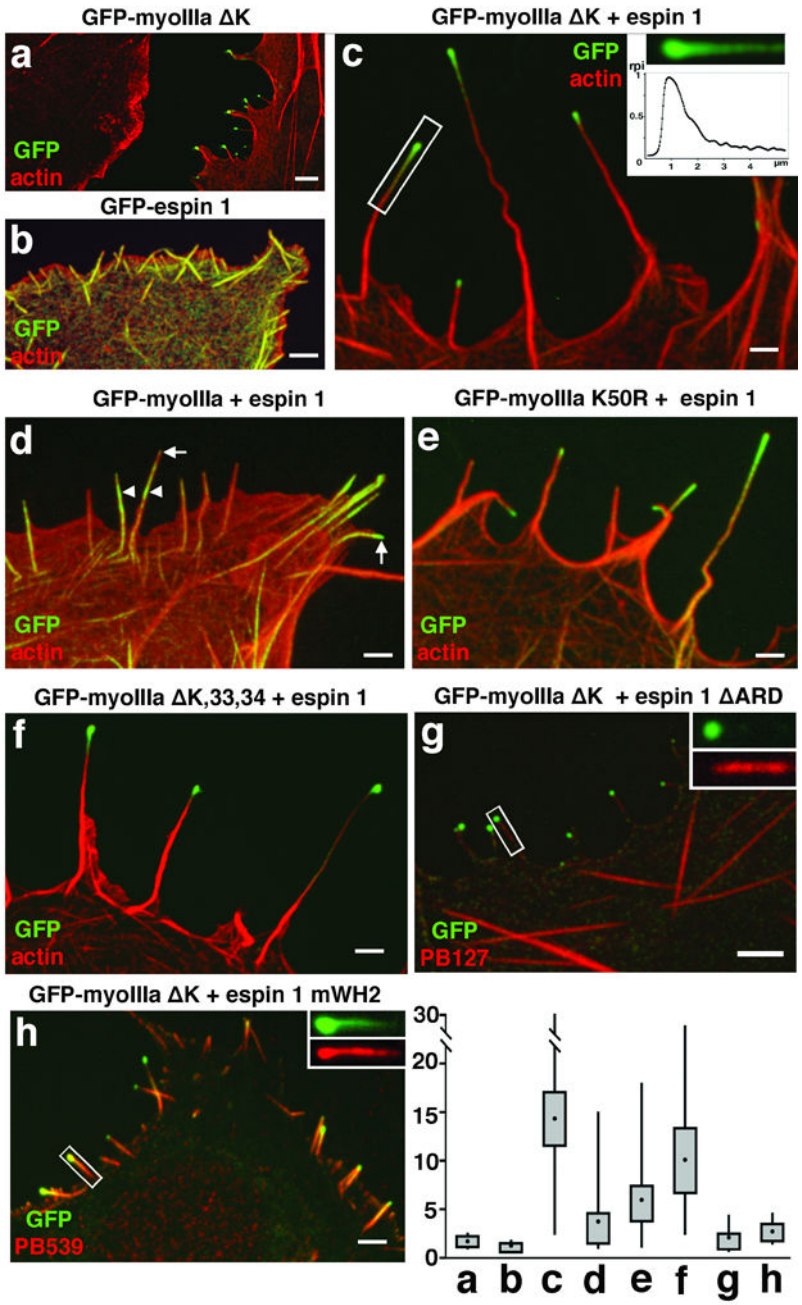

Figure 5.

Myosin IIIa and espin 1 synergistically elongate filopodia in COS-7 cells via espin 1 WH2 activity. Overexpression of either GFP-myoIIIa ΔK (**a**) or GFP-espin 1 (**b**) results in formation of short filopodia (mean lengths = 1.7 ± 0.83 μm and 1.3 ± 0.28 μm, respectively). In contrast, the co-expression of GFP-myoIIIa ΔK (green) and espin 1 (**c**) has a synergistic effect that generates extremely long filopodia (14.3 ± 9.1 μm). F-actin (red) is visualized using Alexa 568-phalloidin. **(inset, c)** Graph of the relative pixel intensity (rpi) of the GFP-myoIIIa ΔK distribution in the single filopodium indicated by the rectangle in **c** shows the

characteristic tip-to-base decaying gradient. (**d**) Co-expression of full length GFP-myoIIIa and espin 1 produces a more limited tip localization of these proteins and elongation of filopodia (3.7 ± 3.2 μm) when compared to co-expression of GFP-myoIIIa ΔK and espin 1. (**e**) The enhanced elongated phenotype is restored to a limited extent (5.93 ± 3.10 μm) when COS-7 cells were co-transfected instead with GFP-myoIIIa K50R and espin 1. **(f)** The enhanced elongation phenotype is similar to **c** when the cell was co-transfected with GFP-myoIIIa ΔK,33,34 and espin 1 (10.02 ± 4.7 μm). (**g**) Co-expression of GFP-myoIIIa ΔK and espin 1 lacking ARD (espin 1 ΔARD, labeled with the pan espin antibody, red) but fails to elongate filopodia (2.05 ± 1.8 μm) and to show tip localization of espin 1 ΔARD **(inset, g)**. **(h)** Co-expression of GFP-myoIIIa ΔK and espin 1 with a mutated WH2 domain (espin 1 mWH2, labeled with espin 1 antibody, red) fails to elongate filopodia (2.65 ± 1.5 μm) despite the fact that espin 1 mWH2 localizes to the tip and forms the tip to base gradient matching the distribution of the GFP-myoIIIa ΔK **(inset, h)**. Scale bars, 2.5 μm. Measurements of filopodia lengths for each of the combinations shown in the panels above are presented as box-plots, with upper and lower whiskers representing the range, the top and bottom of the box representing the upper and lower 25th percentile, and the filled squares represent the mean values.